arXiv:1510.01883v1 [cond-mat.quant-gas] 7 Oct 2015

Enhancing quantum coherence with short-range correlated disorder

P. Capuzzi*
Departamento de Física, Universidad de Buenos Aires, Ciudad Universitaria, Buenos Aires 1428, Argentina and Instituto de Física de Buenos Aires, CONICET, Ciudad Universitaria, Buenos Aires 1428, Argentina

M. Gattobigio† and P. Vignolo‡
Institut Non Linéaire de Nice UMR7335, Université de Nice-Sophia Antipolis, CNRS 1361 route des Lucioles 06560 Valbonne, France

We introduce a two-dimensional short-range correlated disorder that is the natural generalization of the well-known one-dimensional dual random dimer model [Phys. Rev. Lett **65**, 88 (1990)]. We demonstrate that, as in one dimension, this model induces a localization-delocalization transition in the single-particle spectrum. Moreover we show that the effect of such a disorder on a weakly-interacting boson gas is to enhance the condensate spatial homogeneity and delocalisation, and to increase the condensate fraction around an effective resonance of the two-dimensional dual dimers. This study proves that short-range correlations of a disordered potential can enhance the quantum coherence of a weakly-interacting many-body system.

PACS numbers: 67.85.Hj; 71.23.An

I. INTRODUCTION

The presence of impurities usually deeply modify the nature of the spectrum of a quantum system, and thus its coherence and transport properties. In the absence of interactions, if the impurity distribution is completely random, all states of the spectrum are exponentially localized in dimensions one (1D) and two (2D), while a mobility edge exists in dimensions three (3D)[1–3]. If the impurity positions are correlated, as for instance if it exists a minimum distance between the impurities [4, 5], some delocalized states can appear in the spectrum. This was demonstrated in 1D in the context of the Random Dimer Model (RDM) and of the Dual Random Dimer Model (DRDM) [6]. In 1D, the effects of correlated disorder was studied in different physical contexts (see for instance [7–11]). In 2D, the effect of correlations is almost unexplored, except for the case of a speckle potential [12], and for the case of pseudo-2D random dimer lattices with separable dimensions [13]. Correlations in speckle potentials may mimic the presence of a mobility edge [11], but in the thermodynamic limit all states are localized [12]. Random dimers introduce a set of delocalized states in pseudo-2D lattices [13] as in 1D [6]. From a statistical point of view, the main difference between these two models is the decay of the correlation function that is algebraic for the first and exponential for the second. This "short-range" feature of the random dimer model is at the basis of the delocalization mechanism.

In interacting systems, the presence of disordered impurities gives rise to a remarkable richness of phenomena. For instance, the condensate and the superfluid fraction are modified by the presence of the disorder [14, 15], and this can shift the onset of superfluidity [16–18], and, on lattice systems, can induce exotic phases such as the Bose glass [19].

In this work we study the effect of a short-range correlated disorder on a Bose gas confined on a 2D square lattice. First we introduce a 2D generalization of the DRDM (2D-DRDM). In such a model, impurities cannot be first neighbours and each impurity also modifies the hopping with its nearest neighbor sites. Using a decimation and renormalization procedure [20], we show that, in the non-interacting regime, it exists a resonance energy at which the structured impurity is transparent and the states around this energy are delocalized. It is remarkable that this resonance energy does not depend on the system dimensionality and it is the same as the DRDM in 1D [4, 6]. Then, we consider the case of a weakly interacting Bose gas confined on such a potential. Within a Gutzwiller approach, we show that the effect of the 2D-DRDM is to drive the homogeneity of the ground state. The disorder induces a non-monotonic behavior of the condensate spatial delocalization and of the condensate fraction as a function of the disorder strength, and enhances both in correspondence of the resonance energy of 2D-DRDM single-particle Hamiltonian. We show that the dependence of such quantities on the interaction strength can be explained by including the effect of the healing length in the resonance condition discussion.

The manuscript is organized as follows. In Sec. II, we introduce the 2D-DRDM potential and we demonstrate its single-particle delocalization properties in the region of the spectrum around the resonance energy. The effect of such a potential on a weakly-interacting Bose gas is studied in Sec. III, where we also introduce a suitable

*Electronic address: capuzzi@df.uba.ar
†Electronic address: Mario.Gattobigio@inln.cnrs.fr
‡Electronic address: Patrizia.Vignolo@inln.cnrs.fr

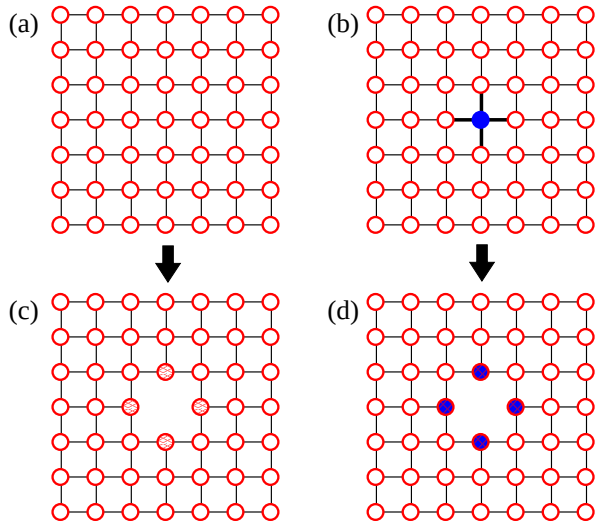

FIG. 1: Schematic representation of (a) the unperturbed Hamiltonian; (b) the Hamiltonian in the presence of a single impurity; (c) the effective Hamiltonian after decimation of the site 0 in the Hamiltonian (a); (d) the effective Hamiltonian after decimation of the site 0 in the Hamiltonian (b).

inverse participation ratio for our many-body system and study it for the case of the 2D-DRDM potential and for an uncorrelated random disorder. Moreover, we compute the density distribution and the condensate fraction as functions of the disorder strength. Our concluding remarks in Sec. IV complete this work.

II. THE DRDM IN TWO DIMENSIONS

We consider the tight-binding single-particle Hamiltonian

$$H = -\sum_{\langle ij\rangle} t_{ij}\left(|i\rangle\langle j| + |j\rangle\langle i|\right) + \sum_{i=1}^{N} \varepsilon_i |i\rangle\langle i| \qquad (1)$$

where ε_i are the on-site energies, t_{ij} the first neighbor hopping terms, N the number of sites and $\langle ij\rangle$ denotes the sum over first neighbor sites.

We focus on a 2D square lattice of linear dimension L ($N = L^2$ lattice sites), and compare the ordered lattice with $\varepsilon_i = 0$ and $t_{ij} = t\ \forall\ \langle ij\rangle$, as schematized in Fig. 1(a) with a lattice where we introduce an impurity at the site 0, $\varepsilon_0 = \Delta$ that modifies the hopping terms involving this site, $t_{0,j} = t'$ [Fig. 1(b)].

A. Effect of correlations in the single-particle spectrum

With the aim of understanding the effect of the impurity, we consider the Green's function $G_{AA}(E) = \langle A|(E-H)^{-1}|A\rangle$ projected on the subspace A, including all sites except the site 0 with coordinates $(0,0)$. Using a decimation and renormalization technique [20], it can be shown that

$$G_{AA}(E) = (E - H_{eff})^{-1} \qquad (2)$$

with

$$H_{eff} = \begin{cases} H_{AA} + \dfrac{t_{0,j}^2}{E-\varepsilon_0} & \text{if } j \text{ is a first}-\text{neighbour site of the site 0} \\ H_{AA} & \text{elsewhere} \end{cases} \qquad (3)$$

where $H_{AA} = \langle A|H|A\rangle$. The effective Hamiltonian for the unperturbed case in Fig. 1 (a), is schematically illustrated in Fig. 1 (c); whereas the effective Hamiltonian for the case with a single impurity in Fig. 1 (b), is illustrated in Fig. 1 (d). The subspace A does not "feel" the presence of the impurity if G_{AA} (H_{eff}) remains the same in the absence or in the presence of the impurity, namely if

$$\frac{t^2}{E} = \frac{(t')^2}{E-\Delta}. \qquad (4)$$

The condition (4) is satisfied if $E = E_{res} = -\dfrac{\Delta}{(t'/t)^2 - 1}$. If E_{res} is an allowed energy of the system, namely if $-4t < E_{res} < 4t$, at $E = E_{res}$ the impurity will not affect the eigenstate at this energy (in the subspace A).

If we add other impurities in the system, as the one in Fig. 1 (b), with the supplementary condition that on-site impurities cannot occupy first neighbor sites (Fig. 2), one can repeat the same argument as above, properly redefining the subspace A, and one obtains exactly the same condition (4) imposing that *all* the N_{imp} impurities do not perturb the system (the subspace A). Thus at $E = E_{res}$, the impurities are transparent as in the 1D DRDM [6]. Indeed, with this procedure, we are defining a 2D-DRDM, where at each "isolated" impurity correspond a structure of 4 hopping terms forming a cross, as shown in Fig. 2. Let us remark that this definition of the model provides the same condition (4) independently from the dimensionality of the system [4, 6]. However our model is fully 2D and the Hamiltonian cannot be mapped onto two 1D DRDM as opposed to Ref. [13].

With the aim of analyzing the localization properties of this model, we consider the Inverse Participation Ratio (IPR)

$$\mathcal{I}(E) = \left\langle \frac{\sum_i |\psi_i(E)|^4}{(\sum_i |\psi_i(E)|^2)^2} \right\rangle. \qquad (5)$$

The symbol $\langle \dots \rangle$ denotes the average over different disorder configurations, and $\psi_i(E)$ the wavefunction on site i and at energy E. If E_α is an eigenvalue of the system and $\psi_i(E = E_\alpha)$ is an extended state, then $\mathcal{I}$ decreases as a function of L. On the other side, if $\psi_i(E_\alpha)$ is a localized state, then $\mathcal{I}$ does not depend on L (if L is larger than the localization length). In Fig. 3 we show the behavior

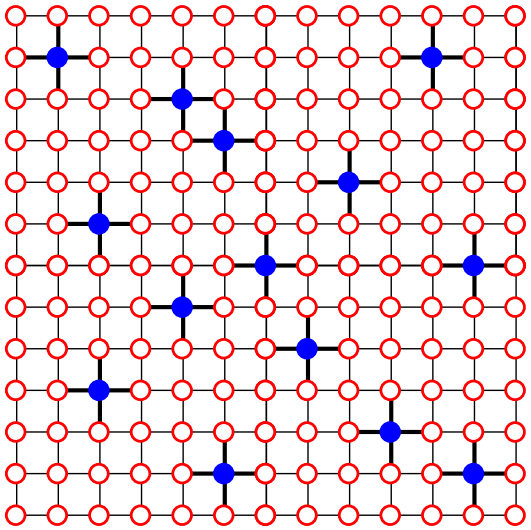

FIG. 2: Schematic representation of the 2D DRDM.

of $\ln(\mathcal{I})$ and $\ln(\mathcal{I}\,L^2)$ (column left and right respectively), for the Hamiltonian illustrated in Fig. 2.

We consider three set of parameters, (i) $\Delta/t = 0.44$ and $t'/t = 1.2$, (ii) $\Delta/t = 3$ and $t'/t = 2$, and (iii) $\Delta/t = 8$ and $t'/t = 3$ that give the same resonance energy, $E_{res}/t = -1$. In all the three cases, the curves $\ln(\mathcal{I}(E)\,L^2)$ collapse around $E = E_{res}$ meaning that the states are delocalized in this energy region. Moreover, due to the large strength of the disorder, the spectrum varies considerably for the cases (ii) and (iii), and an energy gap appears in (iii).

The inverse participation ratio, Eq. (5), in two dimensions has the following asymptotic behavior [21]

$$\lim_{L\to\infty} \mathcal{I}(E) = \begin{cases} 1/L^2 & \text{(extended states)} \\ \text{const.} & \text{(localized states)}\,. \end{cases} \tag{6}$$

Thus, the asymptotic behavior of the function $\mathcal{I}(E)\,L^2$ is

$$\lim_{L\to\infty} \mathcal{I}(E)\,L^2 = L^d\,, \tag{7}$$

with $d = 2$ for localized states, and $d = 0$ for extended states. In Fig. 4 we have analyzed the exponent d as a function of the energy for the set of parameters (iii). We observe a high-energy band of localized states that has been created by the disorder; the original (without noise) band has been distorted, and the states at its boundaries are localized. The center of the band, around E_{res}, is mainly constituted of extended states. The width of the feature around E_{res} corresponds to the width of the resonance dip of the inverse participation ratio at this energy value (Fig. 3).

These results confirm that our 2D extension of the DRDM introduced by Dunlap and collaborators in Ref. [6] for 1D systems introduces a set of delocalized states even at higher dimensions.

III. EFFECTS OF THE INTERACTIONS

We now consider the case of weakly interacting bosons in the presence of the potential defined in Sec. II. This system is described by the Bose-Hubbard Hamiltonian in the grand canonical ensemble

$$H_{BH} = -\sum_{\langle ij\rangle} t_{ij}(\hat{a}_i^\dagger \hat{a}_j + \hat{a}_j^\dagger \hat{a}_i) - \sum_i (\mu - \varepsilon_i)\hat{n}_i + \frac{U}{2}\sum_i \hat{n}_i(\hat{n}_i - 1) \tag{8}$$

where $\hat{a}_i^\dagger$ is the creation operator defined at the lattice site i, $\hat{n}_i = \hat{a}_i^\dagger \hat{a}_i$, U the interparticle on-site interaction strength, and μ denotes the chemical potential fixing the average number of bosons.

We use a Gutzwiller approach to find the ground state wavefunction for a given set of parameters and average number of particles. The Gutzwiller ansatz is given by the site product wavefunction in the occupation number representation

$$|\Phi_{\rm GS}\rangle = \prod_i^{L\times L} \sum_{n_i} f_i(n_i)|n_i\rangle, \tag{9}$$

where $f_i(n_i)$ are the probability amplitudes of finding n_i particles on site i. The ansatz provides an interpolating approximation correctly describing both the Bose-condensed and Mott-insulating phases for low and high U, respectively, in dimensions larger than one. In addition, the approximation becomes exact for all U in the limit of infinite dimensions [22, 23].

We minimize the average energy given by Hamiltonian (8) as a function of the set of amplitudes $f_i(n_i)$ with the normalization and average number of particle constraint for at least 30 disorder realizations for each set of parameters. The minimization is done using standard conjugate-gradient and/or Broyden-Fisher techniques [24] which provides reasonable performance for moderate lattice sizes.

A. Characterization of the condensate delocalization

To quantify the extent of delocalization of the ground state $|\Phi_{\rm GS}\rangle$ in the interacting regime, we decompose it onto the localized basis $|\psi_i\rangle$, $|\Phi_{\rm GS}\rangle = \sum_i c_i|\psi_i\rangle$, representing the distribution of a homogeneous condensate with average density n on the lattice [25]. We define the many-body ground-state IPR $\mathcal{I}_{\rm GS}$ with respect to this basis as

$$\mathcal{I}_{\rm GS} = \left\langle \frac{\sum_{i=1}^{N} c_i^4}{(\sum_{i=1}^{N} c_i^2)^2} \right\rangle. \tag{10}$$

$\mathcal{I}_{\rm GS}$ measures the homogeneity of the ground state in the condensation regime: the smaller $\mathcal{I}_{\rm GS}$ the more spatially delocalized is the condensate.

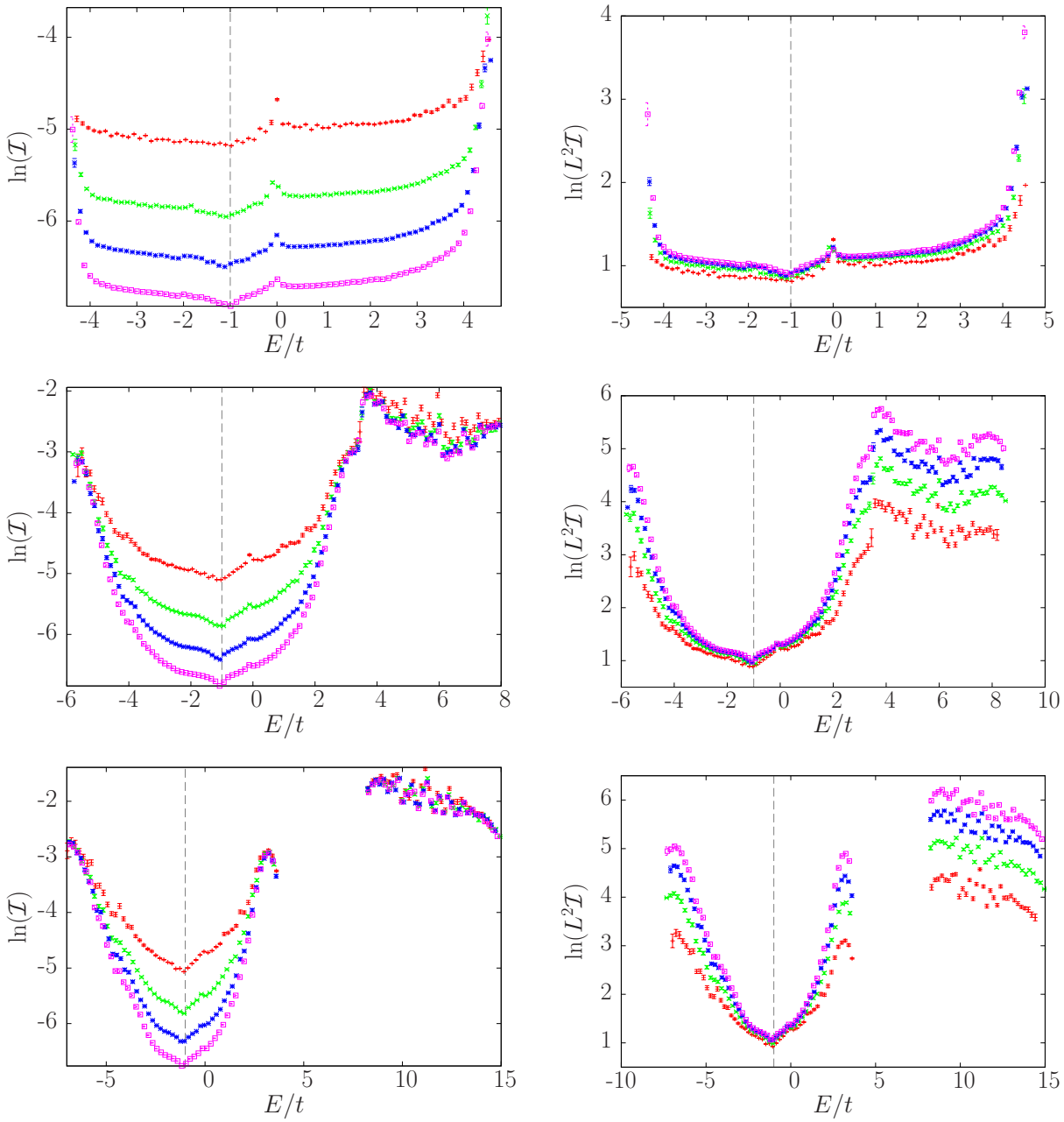

FIG. 3: (Color online) Inverse participation ratio ($\ln(\mathcal{I})$ left column and $\ln(\mathcal{I}\,L^2)$ right column) as a function of the energy E in units of t. The plots in the first row correspond to $\Delta/t = 0.44$ and $t'/t = 1.2$; in the second row correspond to $\Delta/t = 3$ and $t'/t = 2$; and in the the third row to $\Delta/t = 8$ and $t'/t = 3$. The different curves in each plot correspond to different system sizes: $L = 20$ (red), 30 (green), 40 (blue) and 50 (magenta). Each curve correspond to $N_{imp}/N \simeq 0.15$ and to an average over 50 configurations. The data are binned in 80 (first row) and 110 bins (second and third rows). The vertical dashed lines indicate E_{res}.

In Fig. 5 we show the behavior of $\mathcal{I}_{\rm GS}$ as a function of Δ, by fixing $L = 20$, $U/t = 10^{-2}$ and $n = 20$, for several values of t'. We compare the case of 22% of correlated impurities N_{imp} with the one of the same percentage of uncorrelated impurities, where there is no restriction for the position distribution of the on-site impurities Δ and no correlations between them and the additional hopping t' (UN-RAND). We note that due to the correlations present in the 2D-DRDM the maximum percentage of allowed impurities is 50% (in this limit the system would be an ordered checkerboard). We can observe that, in the case of the 2D-DRDM potential, $\mathcal{I}_{\rm GS}$ has a minimum

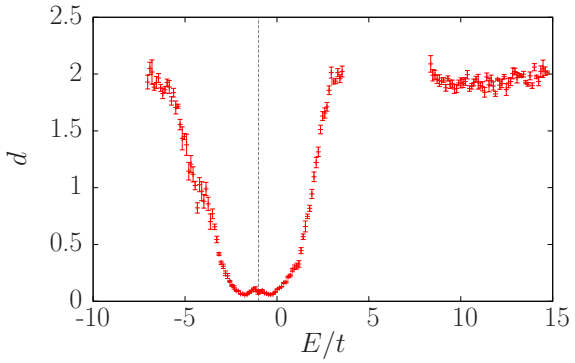

FIG. 4: The exponent of Eq. (7) as a function of the energy for $\Delta/t = 8$ and $t'/t = 3$. The exponent has been obtained using calculations for lattice-linear dimensions $L = 40, 50, 60, 70, 80, 90, 100$ averaged over 20 realizations, the error bars correspond to the standard deviation of the fit of the data to Eq. (7). The vertical dashed line indicates E_{res}.

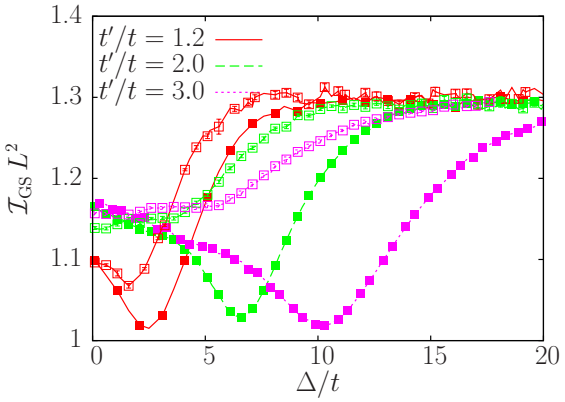

FIG. 5: (Color online) $\mathcal{I}_{\rm GS} L^2$ as a function of Δ/t for $L = 20$, $U/t = 10^{-2}$ and $n = 20$ particles per site. The different curves correspond to different values of t' as indicated in the figure. The filled symbols correspond to the 2D-DRDM potential and the empty symbols correspond to the UN-RAND potential.

as a function of Δ, whose position depends on the value of t'. This non-monotonic behavior is a signature of the resonance induced by the correlations of the disordered potential. Indeed, it disappears for the case of the UN-RAND potential and for large values of t' (strong disorder). The dip in the $\mathcal{I}_{\rm GS}$ for the UN-RAND potential and weak disorder ($t'/t = 1.2$) indicates that some DRDM impurities may still statistically appear, in the absence of correlations. The effect of such impurities is not fully destroyed by the other defects only if the strength of the disorder is weak.

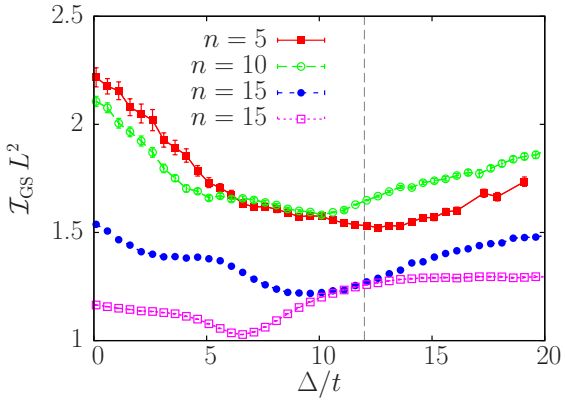

FIG. 6: (Color online) $\mathcal{I}_{\rm GS} L^2$ as a function of Δ/t for $L = 20$, $U = 10^{-2}t$ and $t'/t = 2$. The different curves correspond to different values of the average density n as indicated in the figure. All the curves correspond to the 2D-DRDM potential. The vertical dashed line indicates the non-interacting resonance condition given in Eq. (11).

1. *The resonance effect as a function of the interactions*

In the perturbative regime for negligible interactions, one would expect that correlations modify the ground state if $E_{res} = E_{\rm GS}$, $E_{\rm GS}$ being the ground-state energy per particle, which corresponds to $\simeq -4t$ in the weak disorder regime. This condition, that can be written

$$\Delta = 4t[(t'/t)^2 - 1], \tag{11}$$

determines the location of the minimum of $\mathcal{I}_{\rm GS}$ at $\Delta/t = 1.67$ for $t'/t = 1.2$, $\Delta/t = 12$ for $t'/t = 2$, and $\Delta/t = 32$ for $t'/t = 3$. However, in the limit of strong disorder, due to the interactions these values strongly differ from those shown in Fig. 5. In fact, we calculate $\mathcal{I}_{\rm GS}$ for smaller values of n and verify that the minimum location of $\mathcal{I}_{\rm GS}$ depends on E_{res} and that the shift observed is indeed an effect of the interactions. The results are illustrated in Fig. 6, where we focus on the case $t'/t = 2$. By decreasing the value of n, the minimum position Δ_{min}/t of $\mathcal{I}_{\rm GS}$ shifts from 6.5 to about 12 as expected by the perturbative argument. This shift can be understood as follows. The interactions introduce the so-called healing length $\xi = \sqrt{t/(2nU)}$ [26] that represents a coherence length over which the system feels the effect of an impurity, or in other words, the distance a site affects its neighborhood. For $U/t = 10^{-2}$ and n from 20 to 5, the value of ξ ranges approximately from 1.5 to 3 lattice spacing ℓ, which shows that, already for this U value, the role of the interactions is important, effectively reducing the coherence length. To quantify this effect, we can partition the system into independent boxes of dimension $\xi \times \xi$, and use a mode-matching argument to determine their ground states: the condensate is more homogeneous if the lowest eigenvalue of each box is the same despite the presence of an impurity.

Therefore, this mode-matching argument fixes the

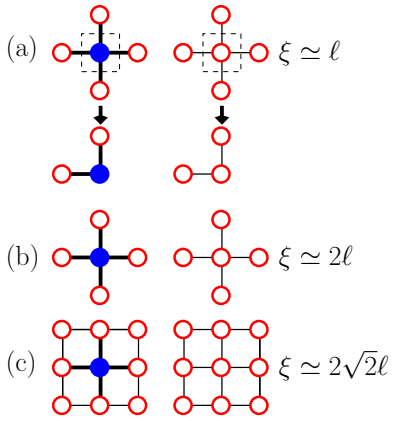

FIG. 7: (Color online)"Boxes" of different sizes, in the presence and in the absence of an impurity.

TABLE I: Effective linear dimensions ξ and positions of the expected resonance Δ for the weakly interacting bosons in the 2D-DRDM.

ξ	Fig.	Δ
ℓ	7(a)	$\sqrt{2}t\,[(t'/t)^2-1]$
2ℓ	7(b)	$2t\,[(t'/t)^2-1]$
$2\sqrt{2}\ell$	7(c)	$2\sqrt{2}t[(t'/t)^2-1]$

value of Δ. For the case $U/t = 10^{-2}$ and $n = 20$, $\xi \simeq 1.6\ell$, and this gives $4.24 < \Delta/t < 6$ while for $n = 5$, $\xi \simeq 3.2\ell$, and we expect to find $8.4 < \Delta/t < 12$, in good agreement with the results showed in Fig. 6. Namely, the larger is ξ, the better we recover the non-interacting condition Eq. (11). This effect is summarized in Table I.

We remark that this mode-matching condition is equivalent to match the resonance energy E_{res} with the lowest eigenvalue of the unperturbed system of size $\xi \times \xi$. These simple arguments, allow us to understand the shift of Δ as a function of the interaction energy Un and the role of the structured impurities in the presence of the interactions.

2. *The resonance effect as a function of the system size*

We study the scaling behavior of $\mathcal{I}_{\rm GS}L^2$ with respect to L. Analogously to the case of the single-particle IPR $\mathcal{I}(E)$ [see Eq. (7)], we expect that

$$\lim_{L\to\infty} \mathcal{I}_{\rm GS}\, L^2 = L^d\,, \tag{12}$$

with $d = 2$ for a condensate localized on few sites, and $d = 0$ for a homogeneous extended condensate. The behavior of $\mathcal{I}_{\rm GS}L^2$ for different values of L is shown in Fig.

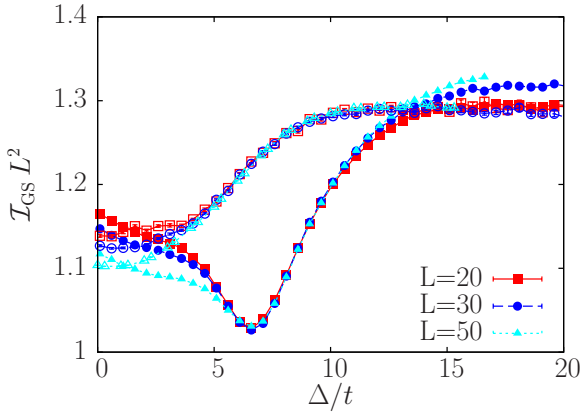

FIG. 8: (Color online) $\mathcal{I}_{\rm GS}L^2$ as a function of Δ/t for $t'/t = 2$, $U/t = 10^{-2}$ and $n = 20$ particles per site. The different curves correspond to different values of L as indicated in the figure. The filled symbols correspond to the 2D-DRDM potential and the empty symbols correspond to the UN-RAND potential.

8. We observe that the minima, corresponding to different system sizes, collapse all together, meaning that the ground state corresponds to a spatial homogeneous condensate in the parameter regime where the correlations are dominant. At lower values of Δ, $\mathcal{I}_{\rm GS}L^2$ scales as $L^{-\epsilon}$, and larger values of Δ, $\mathcal{I}_{\rm GS}L^2$ scales as $L^{\epsilon'}$, with ϵ and $\epsilon' > 0$. This sort of "super-delocalization", in the low Δ region, is determined by the large value of t' that compensates, in the structured impurities, the effect of the site defect. Indeed, we observe an analogous behavior for the UN-RAND potential. For such a potential, where the effect of t' is no more dominant, all the curves collapse together. Thus we expect that in this region the effect of the uncorrelated impurities on the ground state density distribution does not depend on the system size.

B. Condensate delocalization and condensate fraction

With the aim of characterizing the ground state configurations in the different regions, we show in Figs. 9–11 the spatial density distribution n_i for $L = 20$, $n = 20$ at $\Delta/t \simeq 2$ (Fig. 9), $\Delta/t \simeq 6.6$ (Fig. 10), and $\Delta/t \simeq 15$ (Fig. 11) together with a pattern showing the locations of impurities.

The addition of a hopping term t' favors the delocalization of the density both for the 2D-DRDM and UN-RAND disorders. However, in the case of the 2D-DRDM, it is more beneficial as it tends to partially compensate the decrease in the density caused by the site impurity, reducing the decrease by means of the structured disorder. For small values of Δ (see Fig. 9), in the region where the effect of t' is dominant, the density in the impurity regions is even larger with respect to the density elsewhere. For large values of Δ (see Fig. 11), the effect of both types of disorder is similar as the change in the on-

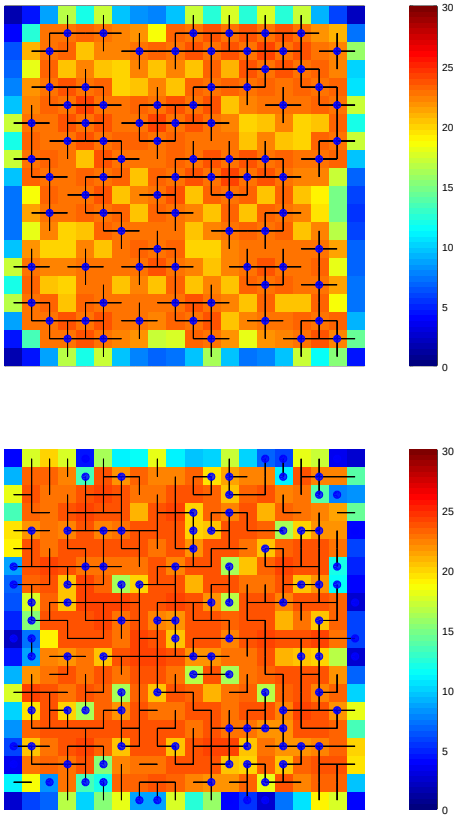

FIG. 9: (Color online) Lattice density plots together with site and bond impurities locations for $t'/t = 2$, $\Delta/t \simeq 2$ and DRDM disorder (top) and UN-RAND (bottom).

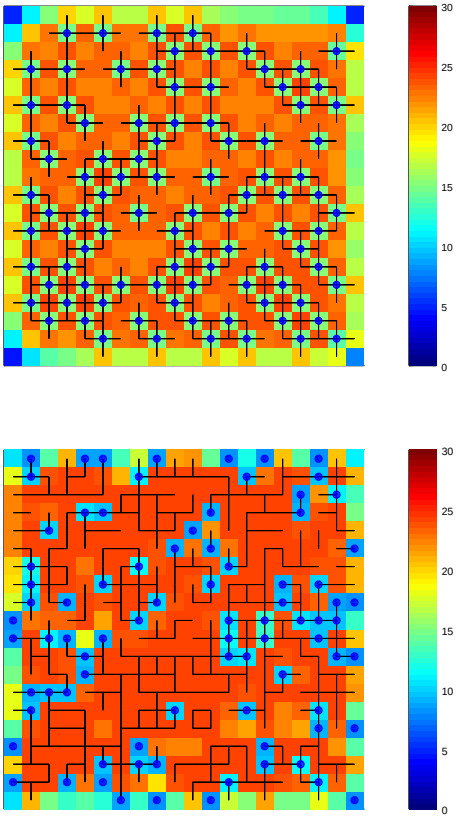

FIG. 10: (Color online) Same as Fig. 10 for $\Delta/t = 6.6$.

site energies dominates. This limit gives rise to a strongly depleted density at the impurity location plus a rather uniform background. The largest differences among the 2D-DRDM and UN-RAND results are seen at the minimum of $\mathcal{I}_{\rm GS}$ (see Fig. 10), where we can clearly observe a more homogeneous density spread over the lattice (lower $\mathcal{I}_{\rm GS}$), and a consequently larger delocalization for the 2D-DRDM than for the UN-RAND potential.

The density behavior determines the condensate fraction $n_c = \sum_i |\langle\Phi_{\rm GS}|a_i|\Phi_{\rm GS}\rangle|^2/n$, as shown in Fig. 12. In correspondence of the minimum of the function $\mathcal{I}_{\rm GS}$, we observe that the condensate fraction n_c does not depends of the system size, in the presence of the 2D-DRDM potential. The resonance condition minimizes the fluctuations with respect the chosen homogeneous basis $|\psi_i\rangle$ and fixes n_c. At lower value of Δ, we observe a "super-delocalization" ($\mathcal{I}_{\rm GS}L^2$ scales as $L^{-\epsilon}$), and for both the 2D-DRDM and the UN-RAND potentials, the large value of t' enhances the coherence and n_c increases with system size.

At larger values of Δ, where $\mathcal{I}_{\rm GS}L^2$ scales as $L^{\epsilon'}$, the 2D-DRDM impurities create holes in the system, and n_c decreases with system size. For the case of the UN-RAND potential, one can observe a monotonic behavior of n_c as a function of Δ. As for the case of the 2D-DRDM, the region where all the curves $\mathcal{I}_{\rm GS}L^2$ collapse together corresponds to a region where n_c does not depend on the system size. The difference with the 2D-DRDM is a larger decrease of n_c in this region. For 2D-DRDM, only one value of Δ has this peculiarity, and the maximum position of the condensate fraction foregoes this point. Let us remark that the minimum of $\mathcal{I}_{GS}$ corresponds to the minimum deviation with respect a homogeneous condensate, and, because of border effects, this target state is not necessarily the one that ensures a maximum value of n_c in finite systems.

The predicted condensate fraction enhancement for the DRDM at low Δ, being it very small, could be very difficult to be measured. However the non-diminishing of the coherence in a range of about 5Δ should be observable, and could be directly compared with the result for the UN-RAND where the decrease of the coherence should be sizable.

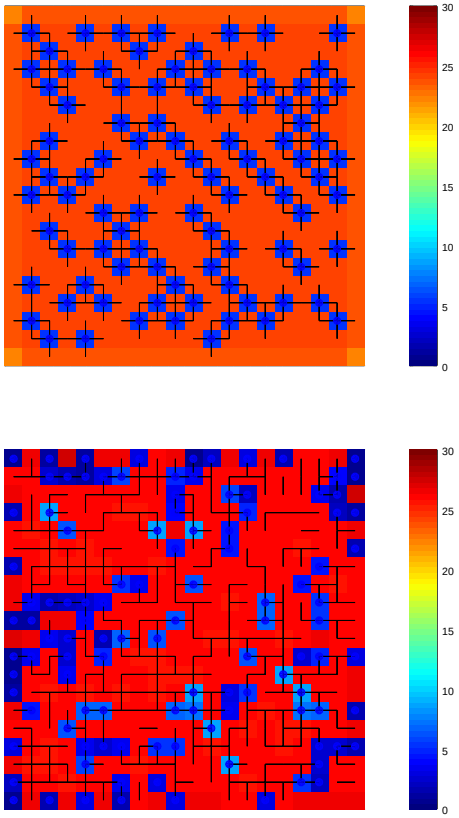

FIG. 11: (Color online) Same as Fig. 10 for $\Delta/t = 15.1$.

IV. CONCLUSIONS

In summary, we introduce a correlated disorder model that is the natural extension of the DRDM in 2D. We show that, in the non-interacting regime, such a disorder introduces some delocalized states if the resonance energy characterizing these structures belongs to the spectrum of the unperturbed system. In the presence of weak interactions, the 2D-DRDM drives the density spatial fluctuations. By means of a mode-matching argument that includes the effect of the interactions, we show that the resonance energy is at the origin of these phenomena. A direct consequence is a non-monotonic behavior of the condensate fraction as a function of the disorder strength, and its enhancement for values close to the resonance condition. This work shows that short-range correlations in a disordered potential can modify and enhance the coherence of a many-body system in the weak interacting regime. Such effects could be measured in the context of ultracold atoms with an accurate measurement of the density and coherence, via, for instance, a fringes contrast interference experiment. Our results could also be extended to homogeneous systems provided one is able to engineer suitable impurities that are transparent for a given energy.

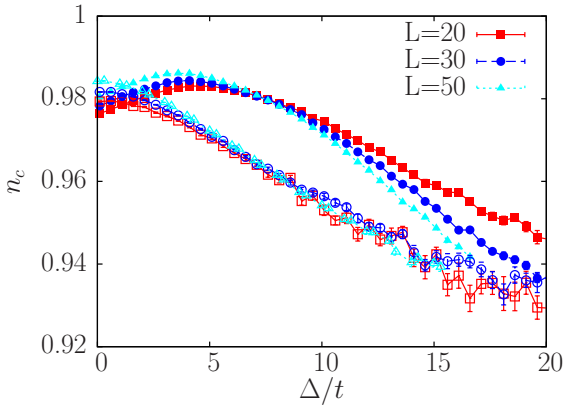

FIG. 12: (Color online) Condensate fraction n_c as a function of Δ/t for $t'/t = 2$, $U/t = 10^{-2}$ and $n = 20$ particles per site. The different curves correspond to different values of L as indicated in the figure. The filled symbols correspond to the 2D-DRDM potential and the empty symbols correspond to the UN-RAND potential.

Acknowledgments

This work was supported by CNRS PICS grant No. 05922. PC acknowledges partial financial support from ANPCyT grant PICT 2011-01217.

[1] P. W. Anderson, Phys. Rev. **109**, 1492 (1958).
[2] E. Abrahams, P. W. Anderson, D. C. Licciardello, and T. V. Ramakrishnan, Phys. Rev. Lett. **42**, 673 (1979).
[3] E. Akkermans and G. Montambaux, *Mesoscopic physics of electrons and photons* (Cambridge University Press, New York, 2007).
[4] J.-F. Schaff, Z. Akdeniz, and P. Vignolo, Phys. Rev. A **81**, 041604 (2010), URL `http://link.aps.org/doi/10.1103/PhysRevA.81.041604`.
[5] M. Larcher, C. Menotti, B. Tanatar, and P. Vignolo, Phys. Rev. A **88**, 013632 (2013), URL `http://link.aps.org/doi/10.1103/PhysRevA.88.013632`.
[6] D. H. Dunlap, H.-L. Wu, and P. W. Phillips, Phys. Rev. Lett. **65**, 88 (1990).
[7] F. A. B. F. de Moura and M. L. Lyra, Phys. Rev. Lett. **81**, 3735 (1998).
[8] F. M. Izrailev and A. A. Krokhin, Phys. Rev. Lett. **82**, 4062 (1999), URL `http://link.aps.org/doi/10.1103/PhysRevLett.82.4062`.
[9] L. Tessieri, J. Phys. A: Math. Gen.Phys. **35**, 9585 (2002).
[10] U. Kuhl, F. M. Izrailev, and A. A. Krokhin, Phys. Rev. Lett. **100**, 126402 (2008).
[11] P. Lugan, A. Aspect, L. Sanchez-Palencia, D. Delande, B. Grémaud, C. A. Müller, and

C. Miniatura, Phys. Rev. A **80**, 023605 (2009), URL http://link.aps.org/doi/10.1103/PhysRevA.80.023605.

[12] R. C. Kuhn, O. Sigwarth, C. Miniatura, D. Delande, and C. A. Müller, New J. Phys. **9** (2007).

[13] U. Naether, C. Mejia-Cortés, and R. A. Vicencio, Phys. Lett. A **379**, 988 (2015).

[14] G. E. Astrakharchik, J. Boronat, J. Casulleras, and S. Giorgini, Phys. Rev. A **66**, 023603 (2002), URL http://link.aps.org/doi/10.1103/PhysRevA.66.023603.

[15] P. Buonsante, F. Massel, V. Penna, and A. Vezzani, Phys. Rev. A **79**, 013623 (2009), URL http://link.aps.org/doi/10.1103/PhysRevA.79.013623.

[16] S. Pilati, S. Giorgini, M. Modugno, and N. Prokof'ev, New Jour. Phys. **12**, 073003 (2010).

[17] T. Plisson, B. Allard, M. Holzmann, G. Salomon, A. Aspect, P. Bouyer, and T. Bourdel, Phys. Rev. A **84**, 061606 (2011), URL http://link.aps.org/doi/10.1103/PhysRevA.84.061606.

[18] B. Allard, T. Plisson, M. Holzmann, G. Salomon, A. Aspect, P. Bouyer, and T. Bourdel, Phys. Rev. A **85**, 033602 (2012), URL http://link.aps.org/doi/10.1103/PhysRevA.85.033602.

[19] M. P. A. Fisher, P. B. Weichman, G. Grinstein, and D. S. Fisher, Phys. Rev. B **40**, 546 (1989), URL http://link.aps.org/doi/10.1103/PhysRevB.40.546.

[20] R. Farchioni, G. Grosso, and G. Pastori Parravicini, Phys. Rev. B **45**, 6383 (1992).

[21] N. C. Murphy, R. Wortis, and W. A. Atkinson, Phys. Rev. B **83**, 184206 (2011).

[22] D. Rokhsar and B. Kotliar, Phys. Rev. B **44**, 10328 (1991), ISSN 0163-1829, URL http://prb.aps.org/abstract/PRB/v44/i18/p10328_1.

[23] W. Metzner and D. Vollhardt, Helv. Phys. Acta **63**, 364 (1990).

[24] W. H. Press, S. A. Teukolsky, W. T. Vetterling, and B. P. Flannery, *Numerical Recipes 3rd Edition: The Art of Scientific Computing* (Cambridge University Press, 2007), ISBN 0521880688.

[25] F. Dukesz, M. Zilbergerts, and L. Santos, New Jour. of Phys. **11**, 043026 (2009).

[26] M. Bukov and L. Pollet, Phys. Rev. B **89**, 094502 (2014), URL http://link.aps.org/doi/10.1103/PhysRevB.89.094502.